Mechanical Systems and Signal Processing 156 (2021) 107669

Contents lists available at ScienceDirect

Mechanical Systems and Signal Processing

journal homepage: www.elsevier.com/locate/ymssp

High-accuracy incident signal reconstruction for in-situ ultrasonic measurement of oil film thickness

Pan Dou [a], Yaping Jia [a], Tonghai Wu [a,*], Zhongxiao Peng [b], Min Yu [c], Tom Reddyhoff [c]

[a] Key Laboratory of Education Ministry for Modern Design and Rotor-Bearing System, Xi'an Jiaotong University, Xi'an, Shaanxi 710049, PR China
[b] School of Mechanical and Manufacturing Engineering, The University of New South Wales, Sydney 2052, Australia
[c] Department of Mechanical Engineering, Imperial College London, London SW7 2AZ, United Kingdom

ARTICLE INFO

Article history:
Received 31 July 2020
Received in revised form 28 November 2020
Accepted 17 January 2021
Available online 11 February 2021

Keywords:
Ultrasonic measurement
Oil film thickness
Incident signal
High-accuracy reconstruction

ABSTRACT

The oil film thickness in an oil-lubricated tribo-pair can be measured using reflected ultrasonic waves and various transformation models. Conventionally, this approach requires the incident signal to be calibrated using off-line methods prior to testing, and this limits the on-line measurement of oil film thickness in sliding components such as journal bearings. To enable on-line calibration, we propose a method of reconstructing the incident signal from the easily obtained reflected signal. This involves analyzing the amplitude and phase spectrum of the reflection coefficient to reconstruct the incident signal. More specifically, the following main findings of the amplitude and phase of reflection coefficient at the resonance frequency are reported. 1) There is a zero-crossing at the resonance frequency, and therefore the phases of the incident and reflected signal are the same. 2) If part of the reflected signal is included for calculation, the frequency of the extreme point in the amplitude spectrum of the reflected signal is equal to the resonance frequency only when the extreme point phenomenon occurs at the center frequency of the transducer. At other positions, the frequency of the minimum amplitude in the amplitude spectrum of the reflected signal is not equal to the resonance frequency. Utilizing these relationships, the phase and amplitude of the incident signal can be accurately reconstructed by following the proposed method, provided the thickness of the oil film between the tribo-pairs can be widely ranged to cover both the blind and the resonance zones. Correspondingly, a practical schedule for the on-line reconstruction of the incident signal is proposed, which includes an operation to adjust the oil film thickness within the blind and the resonance zone. This method is validated on a test rig by comparing it with the traditional off-line methods.

1. Introduction

The thin oil layer between tribo-pairs plays an important role in separating and lubricating moving parts, e.g. sliding bearings and seals, to minimize the wear and extend the service life. There is no doubt that timely information on the oil film thickness would be helpful in providing early warning of failures and preventing needless maintenance. However, the measurement of oil film thickness has so far eluded widespread industrial use due to difficulties in accessing micro-scale and

* Corresponding author.
E-mail address: wt-h@163.com (T. Wu).

https://doi.org/10.1016/j.ymssp.2021.107669
0888-3270/

Nomenclature

Symbol	
$R_n(f)$	reflection coefficient when the number of echoes is n
$R(f)$	specific reflection coefficient when the number of echoes n approaches infinity
$\|R_n(f)\|$	amplitude of the reflection coefficient when the number of echoes is n
$\|R(f)\|$	amplitude of the specific reflection coefficient when the number of echoes n approaches infinity
$B_1(f), \cdots, B_n(f)$	1st, 2nd, ..., nth components of reflected signal
$B(f)$	overall reflected signal from the oil layer including all the echoes
$\|B(f)\|$	amplitude of the overall reflected signal from the oil layer
$I(f)$	incident signal
$\|I(f)\|$	amplitude of the incident signal
$\Phi_{R_n}(f)$	phase of the reflection coefficient when the number of echoes is n
$\Phi_R(f)$	phase of the specific reflection coefficient when the number of echoes n approaches infinity
$\Phi_B(f)$	phase of the reflected signal from the oil layer
$\Phi_I(f)$	phase of the incident signal
$V_{ij}(i,j=1,2,3)$	reflection coefficients at the interfaces where ultrasonic wave transmits from the medium j into medium i
$W_{ij}(i,j=1,2,3)$	reflection coefficients at the interfaces where ultrasonic wave transmits from the medium j into medium i
$z_i(i=1,2,3)$	acoustic impedance of the medium i
f_m	resonance frequency the m-th mode
f_c	center frequency of the ultrasonic transducer
f_G	center frequency of the Gaussian echo
f_{minR}	frequency of minimum amplitude in reflection coefficient spectrum
f_{minB}	frequency of minimum amplitude in reflected signal spectrum
f_{minc}	frequency of minimum amplitude frequency approximating the actual center frequency most when scanning the amplitude spectrum of reflected signal
α	bandwidth factor of the Gaussian echo
β	amplitude of the Gaussian echo
γ	coefficient corelating with the acoustic impedances of the materials
τ	arrival time of the Gaussian echo
ϕ_G	phase of the Gaussian echo
d	oil film thickness
c	sound speed in the oil layer

enclosed dynamic-contact interfaces. With recent developments in ultrasonic models for oil film thickness estimation, this promising technology is being prepared for application to on-line monitoring for engineering purposes.

For a typical sandwiched structure of a liquid-lubricated tribo-pair, different ultrasonic models in both frequency-domain and time-domain have been developed to calculate the film thickness. Essentially, these models are based on different propagation characteristics of ultrasonic waves in materials. In the frequency domain, the reflection coefficient, that is, the ratio of the reflected signal and the incident signal, is used as the key parameter. By plotting the amplitude and the phase of the reflection coefficient vs the coupled index of frequency and film thickness ($f \cdot d$), typical models can be mapped with their effective zones and the wave features [1]. Among these, the resonance model is applicable to measure thick film thickness using the resonance of the incident and reflected waves [2–5]. The film thickness can be calculated from the resonance frequencies in the amplitude spectrum of the reflection coefficient. Different from the resonance model, the spring model is based on the stiffness of the ultra-thin oil film, which can be represented by the amplitude of the reflection coefficient. The spring model is suitable for measuring the thickness of thin films [4–6]. There is the blind zone of these two models, and the phase model was developed to address this issue. The film thickness in the blind zone can be calculated based on the variation of the phase of reflection coefficient [1,7]. Overall, these frequency-domain models have high robustness for signal noise, but require the pre-estimation of the thickness in order to choose a suitable model.

A time-domain model was reported recently focusing on reflected waves directly [8,9]. Essentially, the reflected wave is approximated by the superposition of signals which are the transformations of the incident signal with varied amplitudes and phases. Therefore, the matching approach is adopted to construct the reflected wave with known waves as the incident wave. With successful matching effects, the thickness can be calculated theoretically. Compared to the models in the frequency-domain, the time-domain model can measure oil film thickness over a wide range because it avoids switching between the (frequency-domain) models which cover different effective ranges.

As described before, knowing the incident signal is necessary for using the existing models to measure oil film thickness. However, the capture of the incident signal remains a difficult task for on-line applications, especially in an assembly part. Generally speaking, the incident signal is obtained by sampling the reflected signal at a steel-air interface when the tribo-pair is disassembled [1,4,5]. This approach is based on the principle that the total-reflection would occur at the steel-air interface. Unfortunately, the requirement of disassembly calibration is inconvenient and impractical for the on-line monitoring applications in an assembled tribo-system.

To address this issue, some efforts are made to gain a further understanding of the signals used in the traditional models. By inspecting the resonance zone in the frequency-domain spectrums (see Fig. 14 in [10]), it is found that the minimum amplitude phenomenon synchronically occurs in spectra of both the reflected signal and the reflection coefficient. The corresponding frequencies where minimum amplitudes occur are denoted as f_{minB} and f_{minR} respectively, as shown in Fig. 1. Therefore, f_{minB}, the frequency at the minimum amplitude in the reflected amplitude spectrum can be directly adopted as the resonance frequency for the resonance model [10]. However, there are non-negligible errors for this method compared with the traditional resonance model (refer to Fig. 8 in [11] and Fig. 15 in [10]).

For the spring model [12], the regression models of the phase and amplitude are constructed between the incident and the reflected signal, respectively. However, the valid zone of the regression relationship is limited with the model. Furthermore, its accuracy is sensitive to the surface roughness of the tribo-pair (see Fig. 18 in [10]). A new regression model was proposed [13] with an enlarged effective range covering both the spring and the blind model zones. An extended Kalman filter algorithm was adopted in this model to estimate the phase and amplitude of the incident signal. However, the problems regarding the accuracy and robustness cannot be ignored (see Figs. 5–7 in [13]).

Recently, a wavelet-based modulus maximum method [14] was introduced by matching the reflected signal with the Mexican wavelets. The transient position of the first two reflected echoes can be determined using the modulus maximum method. Correspondingly, the time difference between these two reflected echoes can be used to calculate the oil film thickness using the time-of-flight method. However, for thin films, the echoes may be superposed seriously in the reflected signal (see Fig. 8(b) in [1]), making it difficult to be determined due to the limitation of the pulse width of the waves. Therefore, this method is merely suitable for thick film measurement (e.g., thickness more than 150 μm using a transducer of 5 MHz center frequency in [14]).

Overall, there are bottlenecks for applying the existing ultrasonic methods for the on-line measurement of oil film thickness without off-line calibrations. To address this issue, an on-line calibration method is investigated for an assembly part by reconstructing the incident signal from the sampled reflected signals directly. The full spectrum-domain features including the blind and the resonance zones are inspected. In particular, the relationship between the reflected and incident signals is investigated. Based on the understanding of this relationship, the phase value and amplitude spectrum of the incident signal are reconstructed from the resonance model and blind zones, respectively. Aiming for on-line application, a comprehensive procedure is designed in which running the object system from the start to the full speed is involved for actual operations.

The remainder of this paper is organized as follows: Section 2 introduces the traditional ultrasonic models. The reconstruction method of the incident signal is described in Section 3. The experimental apparatus and results are presented in Section 4. Section 5 discusses the advantages and disadvantages of the proposed reconstruction method of the incident signal compared with existing methods. Finally, the conclusions are drawn in Section 6.

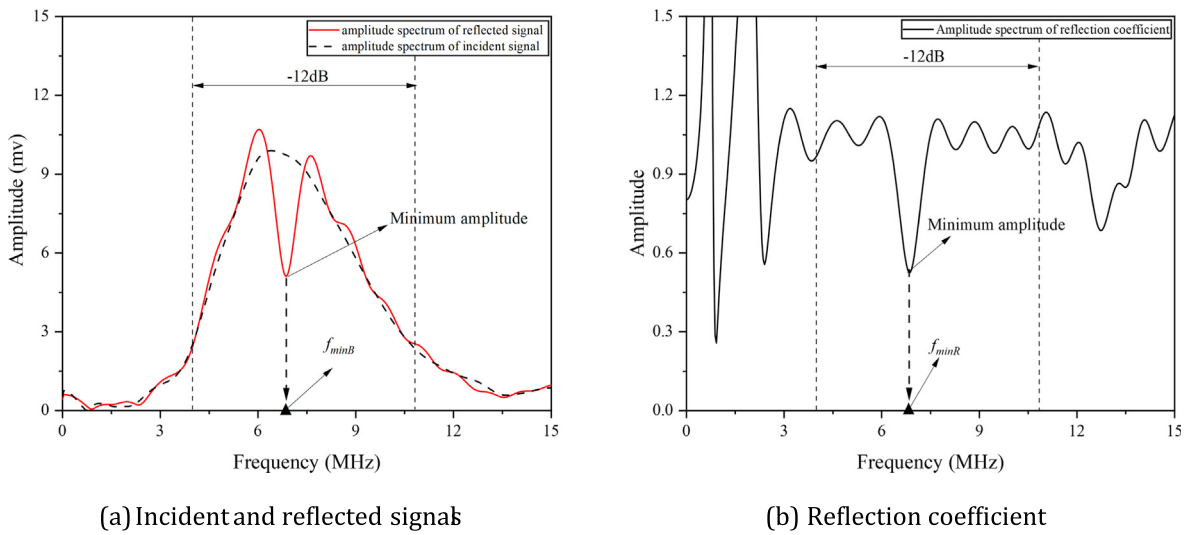

Fig. 1. (a) amplitude spectrum of the incident and reflected signals; (b) amplitude spectrum of reflection coefficient, which is the ratio of the amplitude spectrum of the reflected signal to that of the incident signal.

2. Review of frequency-domain based ultrasonic models

2.1. Ultrasonic reflection coefficient

It is popular to use a three-layered sandwich structure as a simplified model to simulate a tribo-pair with a thin oil film in between for lubrication. The propagation of ultrasonic waves can be described in Fig. 2. The reflection coefficient, $R_n(f)$, is defined to be the proportion between the reflected and incident signals [15,16]:

$$R_n(f) = \frac{B(f)}{I(f)} = \frac{B_1(f) + B_2(f) + \cdots + B_n(f)}{I(f)} = \gamma_1 + \gamma_2 \exp\left(\frac{4i\pi fd}{c}\right) + \gamma_3\left[\exp\left(\frac{4i\pi fd}{c}\right)\right]^2 + \cdots + \gamma_n\left[\exp\left(\frac{4i\pi fd}{c}\right)\right]^{n-1} \quad (1)$$

where, $B(f)$ is the total reflected signals comprising of $B_1(f), \ldots, B_n(f)$, which are the corresponding reflected echoes from the oil layer; $I(f)$ is the incident signal; d is the oil film thickness; c is the sound speed in the oil; and γ is the coefficient correlating with the acoustic impedances of the materials, which can be denoted by Eq. (2).

$$\gamma_i = \begin{cases} V_{12}, & i = 1 \\ \cdots & \\ W_{12}V_{23}^{n-1}V_{21}^{n-2}W_{21}, & i = n \end{cases} \quad (2)$$

where

$$V_{12} = \frac{z_1 - z_2}{z_1 + z_2}, V_{23} = \frac{z_2 - z_3}{z_2 + z_3}, V_{21} = -V_{12}, W_{12} = 1 - V_{12}, W_{21} = 1 + V_{21} \quad (3)$$

where V_{ij} and W_{ij} (i,j = 1,2,3) are the reflection and transmission coefficients, respectively, at the interfaces where ultrasonic wave transmits from the j-th medium into i-th medium. More generally, these can be calculated by:

$$V_{ij} = \frac{z_i - z_j}{z_i + z_j}, W_{ij} = 1 - V_{ij} \quad (4)$$

When n goes to infinity, Eq. (1) can be simplified as:

$$R(f) = \frac{V_{12} + V_{23}\exp(\frac{4i\pi fd}{c})}{1 + V_{12}V_{23}\exp(\frac{4i\pi fd}{c})} \quad (5)$$

And the corresponding theoretical amplitude $|R(f)|$ and phase $\Phi_R(f)$ can be denoted as

$$|R(f)| = \left[\frac{(V_{12} + V_{23})^2 - 4V_{23}V_{12}\sin^2(\frac{2\pi fd}{c})}{(1 + V_{23}V_{12})^2 - 4V_{23}V_{12}\sin^2(\frac{2\pi fd}{c})}\right]^{\frac{1}{2}} \quad (6)$$

$$\Phi_R(f) = \tan^{-1}\left[\frac{V_{23}(1 - V_{12}^2)\sin(\frac{4\pi fd}{c})}{V_{12}\left(1 + V_{23}^2\right) + V_{23}(1 + V_{12}^2)\cos(\frac{4\pi fd}{c})}\right] \quad (7)$$

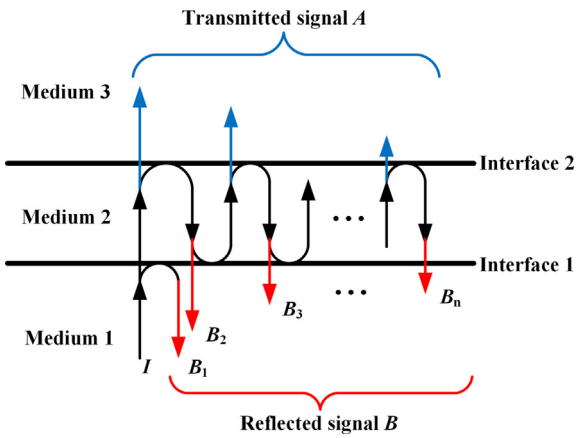

Fig. 2. The diagram of the propagation of ultrasonic waves in a three-layered sandwich system.

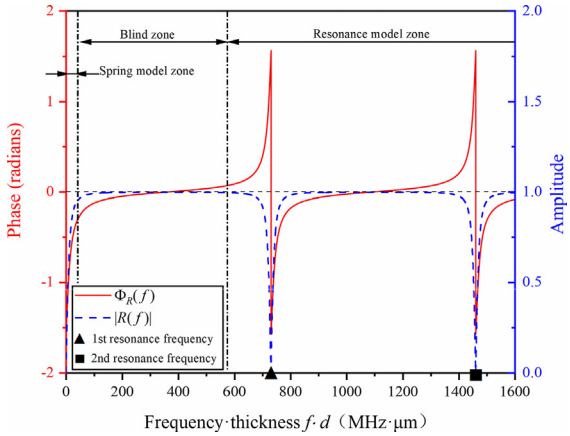

Fig. 3. The theoretical $|R(f)|$ (blue, dotted line) and $\Phi_R(f)$ (red, solid line) of the reflection coefficient in the steel-oil-steel system. The upper limit of the spring model is 40 MHz · μm according to $|R(f)|$ [4], and the lower limit of the resonance model is 500 MHz · μm with the measured minimum thickness of the resonance model 50 μm and the transducer's center frequency is 10 MHz [10].

Based on Eqs. (6) and (7), a typical plot can be made to describe the variation of the reflection coefficient in terms of amplitude and phase spectra ($|R(f)|$ and $\Phi_R(f)$). As shown in Fig. 3, the variations of $|R(f)|$ and $\Phi_R(f)$ with the combination index, $f \cdot d$, are calculated for a steel-oil-steel structure under definite conditions. With a transducer of fixed frequencies, the variation with the oil film thickness can be analysed with different ultrasonic models.

2.2. Ultrasonic models

This section reviews three classical models based on the reflection coefficient: resonance model, spring model, and phase model. To apply these models, the calculation model of the practical reflection coefficient is also reviewed.

2.2.1. Resonance model

The resonance phenomenon between the reflected wave and incident wave will occur when the oil film thickness is integer multiples of the half-wavelength of the ultrasonic wave [4,5]. The oil film thickness d then can be calculated using

$$d = \frac{m\lambda}{2} = \frac{mc}{2f_m} \tag{8}$$

where λ is the wavelength of the ultrasonic wave, m is the mode number of the resonance frequency, f_m is the resonance frequency of the m-th mode.

The resonance model is widely applied in different situations [5,17]. However, there are two issues with this approach:

1) The periodic minimum amplitudes and the even-order zero-crossings of the phase correspond to the resonance frequencies. Therefore, the oil film thickness can be calculated using the resonance model with the identified resonance frequencies (f_m) from the spectrum of the reflection coefficient [17]. However, this fails when f_m falls out of the frequency range of the transducer;

2) When the oil film thickness is in the resonance model zone, the reflected echoes from the oil layer are partially superposed in the time domain and the duration time of the whole reflected echo cluster is long. Due to the interference of reflected echoes from the non-oil layer interface, only partial reflected echoes can be included for the calculation. The principle of wave superposition has been used to analyse the effect of the number of echoes on the resonance model in a previous study [17]. The result shows that the positions of the frequency of minimum amplitude and the zero-crossings are independent of the number of echoes.

2.2.2. Spring model and phase model

In the spring model zone, as can be seen from Fig. 3, the amplitude increases monotonously with the variable $f \cdot d$ when the amplitude is below 0.95 or the index of $f \cdot d$ is below 40 MHz · μm. The oil film thickness can be calculated using this monotonous relationship, the so-called spring model [4,5].

Between the spring model and the resonance model, there is the blind zone in which the amplitude has no significant changes with the index $f \cdot d$. In the previous study [1], it was found that the phase continuously increases in both the blind and spring model zones. Correspondingly, a phase model was proposed in that work (see Fig. 10(b) in [1]).

2.2.3. Calculation model of the reflection coefficient

In the frequency-domain, the above models are based on the reflection coefficient $R(f)$, the amplitude $|R(f)|$ and phase $\Phi_R(f)$ of which can be obtained practically by:

$$|R(f)| = \frac{|B(f)|}{|I(f)|} \tag{9}$$

$$\Phi_R(f) = \Phi_B(f)\text{-}\Phi_I(f) \tag{10}$$

where $|B(f)|$ and $\Phi_B(f)$ are the amplitude and the phase of the reflected wave from the oil layer, respectively; and $|I(f)|$ and $\Phi_I(f)$are the amplitude and the phase of the incident wave $I(f)$, respectively.

It can be seen from Eqs. (9) and (10) that the incident signal $I(f)$is necessary for the calculations. As mentioned above, it is not practical to disassemble the tribo-pair to obtain the incident signal from an assembled tribo-pair, for example the journal bearings in a turbine system. Therefore, the focus is moving to the in-situ capture of the incident signal.

3. Reconstruction of the incident signal

This section reports method for reconstructing the incident signal from the reflected signals. Focusing on the resonance phenomena in the amplitude spectra, the relationship between the two critical frequencies, that is, f_{minB} and f_m are analysed theoretically in Section 3.1. Furthermore, the conditions when the two frequencies are the same are analysed using simulations. The reconstruction principle of the incident signal from the reflected signals is then proposed in Section 3.2. Finally, a flow chart is established for practical implementation in an assembled system in Section 3.3.

3.1. The equivalence condition of f_{minB} and f_m

3.1.1. Theoretical analysis

It has been reported in [10] that, with the observed synchronization of the minimum amplitude in $|B(f)|$ and $|R(f)|$ in the experiment, and therefore it is speculated that f_{minB} may be equal to f_{minR}. If this relationship is valid, f_{minB} could be directly adopted as f_m. An attempt was made to confirm this theoretically with two reflected echoes (denoted by $\boldsymbol{B_1}$ and $\boldsymbol{B_2}$ in Fig. 2) [11]. However, there are an infinite number of echoes reflected from the oil layer and the influences of the echo numbers were not analysed. Further, non-negligible errors, regarded as noise in the referred paper, are introduced by directly substituting f_{minR} with f_{minB} (refer to Fig. 8 in [11] and Fig. 15 in [10]). Therefore, it can be generalized that the relationship between f_{minR} (or f_m) and f_{minB} has not been established, which is also the topic of the current study.

With the n reflected waves, the theoretical amplitude $|R(f)|$ of the reflection coefficient can be derived directly from Eq. (1):

$$|R(f)| = \left(Re^2 + Im^2\right)^{\frac{1}{2}} = \left\{ \begin{array}{c} \gamma_1^2 + \gamma_2^2 + \gamma_3^2 + \cdots + \gamma_n^2 + 2(\gamma_1\gamma_2 + \gamma_2\gamma_3 + \cdots + \gamma_{n-1}\gamma_n)\cos\left(\frac{4\pi fd}{c}\right) + \\ 2(\gamma_1\gamma_3 + \cdots + \gamma_{n-2}\gamma_n)\cos\left(\frac{8\pi fd}{c}\right) + \cdots + 2\gamma_1\gamma_n\cos\left[\frac{4(n-1)\pi fd}{c}\right] \end{array} \right\}^{\frac{1}{2}} \tag{11}$$

If the first derivative $|R'(f{=}f^*)| = 0$ and $|R''(f{=}f^*)| > 0$, $|R(f)|$ will have a minimum value at $f = f^*$. The first and second derivatives of $|R(f)|$ with respect to f are as follows:

$$|R(f)|' = -\frac{4\pi dA(f)}{c|R(f)|} \tag{12}$$

$$|R(f)|'' = -\frac{4\pi d(cA(f)'|R(f)|^2 + 4\pi dA(f)^2)}{c^2|R(f)|^3} \tag{13}$$

where

$$\begin{aligned} A(f) = {} & (\gamma_1\gamma_2 + \gamma_2\gamma_3 + \cdots + \gamma_{n-1}\gamma_n)\sin\left(\frac{4\pi fd}{c}\right) + 2(\gamma_1\gamma_2 + \gamma_2\gamma_3 + \cdots + \gamma_{n-1}\gamma_n)\sin\left(\frac{8\pi fd}{c}\right) + \cdots \\ & + (n-1)\gamma_1\gamma_n\sin\left[\frac{4(n-1)\pi fd}{c}\right] \end{aligned} \tag{14}$$

$$\begin{aligned} A(f)' = {} & \frac{4\pi d}{c}(\gamma_1\gamma_2 + \gamma_2\gamma_3 + \cdots + \gamma_{n-1}\gamma_n)\cos\left(\frac{4\pi fd}{c}\right) + \frac{16\pi d}{c}(\gamma_1\gamma_2 + \gamma_2\gamma_3 + \cdots + \gamma_{n-1}\gamma_n)\cos\left(\frac{8\pi fd}{c}\right) + \cdots \\ & + \frac{4\pi d(n-1)^2}{c}\gamma_1\gamma_n\cos\left[\frac{4(n-1)\pi fd}{c}\right] \end{aligned} \tag{15}$$

Substituting the equation $f_m = mc/2d$ into Eq. (12) and Eq. (13) gives:

$$|R(f_m)|' = 0 \tag{16}$$

$$|R(f_m)|'' > 0 \tag{17}$$

Eqs. (16) and (17) describe the principle of the minimum amplitude phenomenon at f_m in $|R(f)|$. It can be seen that the number of echoes has no influences on f_{minR}, which is consistent with the previous study [17].

From Eq. (9), the amplitude of the reflected signal from the oil layer can be presented as:

$$|B(f)| = |I(f)||R(f)| \tag{18}$$

The differential of Eq. (18) with respect to the frequency is:

$$|B(f)|' = |I(f)|'|R(f)| + |I(f)||R(f)|' \tag{19}$$

Substituting Eq. (19) with f_m, it can be rewritten as:

$$|B(f_m)|' = |I(f_m)|'|R(f_m)| \tag{20}$$

In steel-oil-steel structure, referring to Eq. (6), $|R(f_m)| = 0$ when $n = \infty$, and thus $|B(f_m)|' = 0$. In contrast, $|R(f_m)| \neq 0$ when $n \neq \infty$. In latter case, $|B(f_m)|' = 0$ only when $|I(f_m)|' = 0$. To determine the non-zero value of $|I(f_m)|'$, an incident wave from the transducer can be simplified as a monotone convex function, which has the maximum amplitude at the center frequency of transducer (which is denoted as f_c). Therefore, $|I(f_m)|' = 0$ at f_c. Consequently, it can be concluded that $|B(f_m)|' = 0$ only when $f_m = f_c$.

The two key findings from the above studies are mathematically summarized as follows:

$$\begin{cases} f_{minB} \equiv f_m, & n = \infty \\ f_{minB} = f_m, & n \neq \infty \& f_m = f_c \\ f_{minB} \neq f_m, & n \neq \infty \& f_m \neq f_c \end{cases} \tag{21}$$

3.1.2. Simulation for verification

For verification, the propagation of the ultrasonic waves in a three-layered sandwich system is simulated with a standard incident wave. The material parameters adopted for the simulation are listed in Table I. Considering the bandpass characteristics of the ultrasonic pulse, the incident wave is simulated with Gaussian function as shown below [18].

$$I(t) = \beta e^{-\alpha(t-\tau)^2} \cos(2\pi f_G(t-\tau) + \phi_G) \tag{22}$$

where α is the bandwidth factor, τ is the arrival time, and f_G, ϕ_G, and β are the center frequency, the phase and the amplitude of Gaussian wave$I(t)$, respectively.

The normalized ($\beta = 1$) and zero-phase ($\phi_G = 0$) magnitude spectrum of the incident wave is obtained by Fourier transforming

$$|I(f)| = \frac{1}{2}\sqrt{\frac{\pi}{\alpha}}\left(e^{\frac{-\pi^2(f-f_G)^2}{\alpha}} + e^{\frac{-\pi^2(f+f_G)^2}{\alpha}}\right) \tag{23}$$

By setting bandwidth factor $\alpha = 92.4(\text{MHz})^2$, arrival time $\tau = 0.4\mu s$, and the center frequency $f_G = 6.8$MHz, the simulated magnitude spectrum of the normalized incident wave can be reconstructed. These parameter values are obtained by fitting the Gaussian echo model to the actual reflected signal from a steel-air interface.

The $|B(f)|$ at different thicknesses can be simulated with Eqs. (11), (18) and (23). Fig. 4 shows the results of the oil film thickness of 125 μm, 108 μm, and 95 μm with the numbers of echoes 4, 6, 8, 12, and infinite, respectively.

The resonance phenomena with a minimum amplitude are denoted with the dotted boxes as shown in Fig. 4(a)-(c). It is found that, with the echoes number increasing, the amplitude has a smaller minimum amplitude at the resonance point. From the magnified zones shown in Fig. 4(a)-(c), it is found that f_{minB} varies with the echo numbers. With a definite resonance frequency for an oil layer thickness, f_{minB} shows deviation with different echo numbers. And the deviation tends to zero when the echo number tends to be infinite. This means f_{minB} and f_m is not equivalent even with the same oil layer thickness if the echoes are not completely included.

Practically it is not feasible to include all the reflected echoes to calculate the reflection coefficient mainly due: 1) in terms of data acquisition, the infinity echo waves cannot be fully digitized and captured by a finite time window; 2) The later echoes are significantly attenuated, resulting in low signal-to-noise ratios and thus cannot be accurately measured as shown in the dotted line box of Fig. 5a; 3) in the case of multi-layer structure (especially for those with more than three-layers), where adjacent echo clusters are partly overlapped as shown in Fig. 5(b), it is difficult to isolate each cluster (denoted as A_1) from its adjacent ones.

As an exception, the constant equivalence between the two frequencies can be observed in the enlarged view of Fig. 4(b) in which the minimum amplitude phenomenon occurs at the central frequency of the incident wave 6.8 MHz. The simulated results are consistent with the theoretical analysis. Further error analysis using measured data is conducted and presented in Section 4.

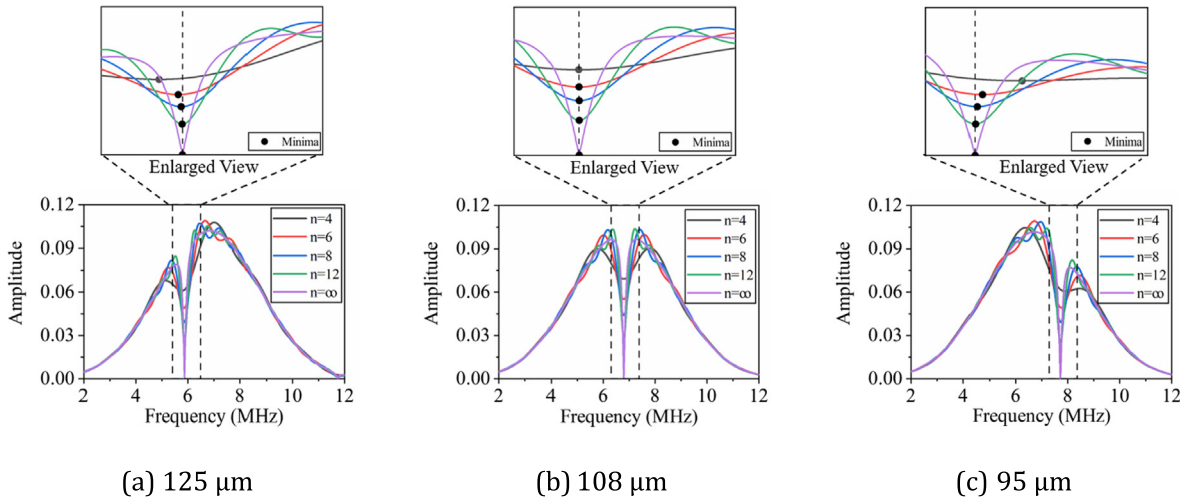

Fig. 4. The $|B(f)|$ at the thickness of (a) 125 μm, (b) 108 μm, and (c) 95 μm; vertical dash lines in the enlarged view represent the position where the resonance phenomenon appears, the frequency of minimum amplitude is always equal to the resonance frequency when minimum amplitude phenomenon appears at f_G (6.8 MHz).

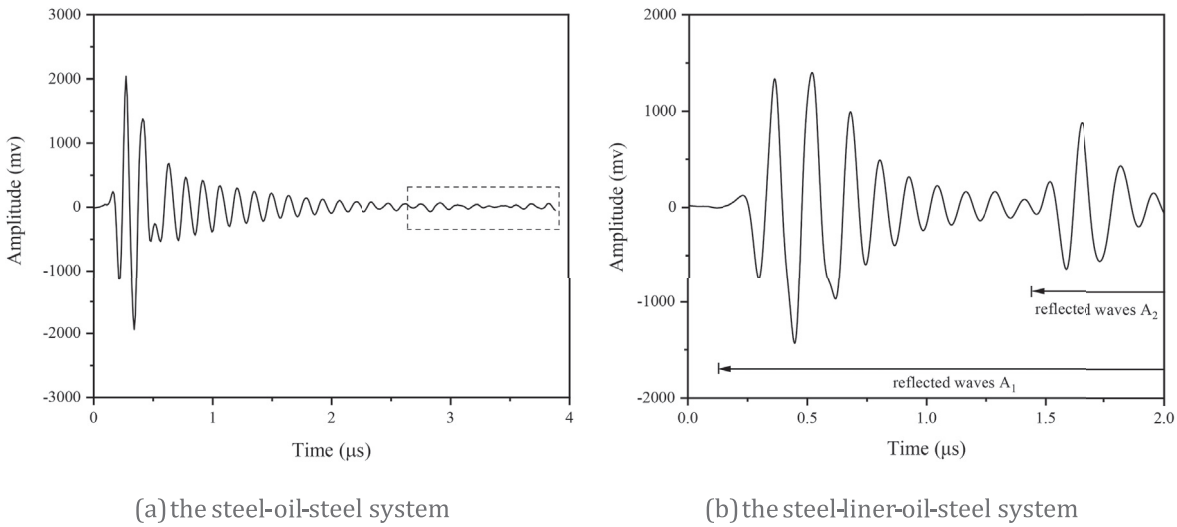

Fig. 5. Plots of the time-domain response of reflected echoes (with oil film thickness within the resonance model zone) from (a) the steel-oil-steel system and (b) the steel-liner-oil-steel system. The center frequency of the utilized transducer is 7 MHz.

3.2. Reconstruction principle of the incident signal

In this section, the constant equivalence phenomenon at f_c between the two frequencies (namely f_{minB} and f_m) is used to reconstruct the phase and amplitude of the incident signal in turn.

3.2.1. Phase reconstruction of the incident signal

1) Method

With the definite number of reflected waves, the theoretical phase of the reflection coefficient can be derived directly from Eq. (1):

$$\Phi_R(f) = \operatorname{atan}\frac{Im}{Re} = \frac{\gamma_2 \sin\left(\frac{4\pi fd}{c}\right) + \gamma_3 \sin\left(\frac{8\pi fd}{c}\right) + \cdots \gamma_n \sin\left[\frac{4(n-1)\pi fd}{c}\right]}{\gamma_2 \cos\left(\frac{4\pi fd}{c}\right) + \gamma_3 \cos\left(\frac{8\pi fd}{c}\right) + \cdots \gamma_n \cos\left[\frac{4(n-1)\pi fd}{c}\right]} \tag{24}$$

Substituting the resonance frequency f_m into the Eq. (24) gives

$$\Phi_R(f_m) = 0 \tag{25}$$

The number of reflected echoes n is not included in Eq. (25), which means that the value of n has no influence on the position of zero-crossing in $\Phi_R(f)$. Further, it can be deduced from the Eq. (10) and (25) that $\Phi_I(f_m) = \Phi_B(f_m)$. It has been proved in the section 3.1 that $f_{minB} = f_m$ when $f_{minB} = f_c$. Therefore, $\Phi_I(f_{minB}) = \Phi_B(f_{minB})$ when $f_{minB} = f_c$.

2) Verification

According to Eq. (10), $\Phi_I(f_{minB}) - \Phi_B(f_{minB}) = -\Phi_R(f_{minB})$. With the identified frequencies of minimum amplitude in the simulated $|B(f)|$ at different oil film thicknesses, the corresponding phases of the reflection coefficient under different number of echoes can be calculated using Eq. (24). The simulation result under different thicknesses and the number of echoes is shown in Fig. 6. The black vertical dash line represents the center frequency (6.8 MHz).

It can be seen that if $n = \infty$, $\Phi_I(f_{minB}) = \Phi_B(f_{minB})$ at the any f_{minB}. If $n \neq \infty$, $\Phi_I(f_{minB}) = \Phi_B(f_{minB})$ only when $f_{minB} = 6.8$MHz. In fact, it is impractical that all the reflected echoes are included for the calculation. Therefore, the reconstruction principle of the phase of the incident signal can be concluded from the above analysis: when the minimum amplitude phenomenon appears at the center frequency of the transducer, the phase of the incident signal can be acquired by referring to that of the reflected signal at $f_{minB} = f_c$ in the absence of the incident signal.

3) Calibration of the center frequency of the transducer

The phase of the incident signal can be acquired only at $f_{minB} = f_c$, but the actual f_c often differs from its nominal value due to the parameter discreteness [20]. Therefore, the actual f_c should be calibrated exactly before the setting. The principle can be illustrated as follows.

Fig. 7 shows the variations of $|B(f)|$ and the theoretical $|R(f)|$ when the oil film thickness just locates at the transition from the blind to the resonance zone. Meanwhile, the amplitude of the corresponding incident wave is also presented for reference. As seen from Fig. 7, the minimum amplitude first appears at the border of transducer bandwidth while the theoretical $|R(f)|$ remains in the blind zone. It means that the peak frequency in the $|B(f)|$ is basically equal to the actual f_c. This provides the basic principle to extract the actual f_c.

3.2.2. The amplitude reconstruction of the incident signal

To obtain the accurate resonance frequencies, the minima frequencies should be extracted from $|R(f)|$. Therefore, the amplitude spectrum of the incident signal needs to be reconstructed to calculate $|R(f)|$.

According to Eq. (9), if the $|B(f)|$ from oil layer at a known thickness can be captured, the theoretical $|R(f)|$ of oil layer at this known thickness can be calculated. Further the amplitude spectrum of the incident signal $|I(f)|$ can be obtained as:

$$|I(f)| = \frac{|B(f)|}{|R(f)|} \tag{26}$$

For the reflected signal in the resonance zone, when the frequency of minimum amplitude occurs at the actual f_c, the oil film thickness can be calculated accurately using the resonance model. However, it is difficult to calculate the theoretical $|R(f)|$ by Eq. (11) because the exact number of echoes cannot be obtained with echoes partially superposed (see Fig. 8(a) in [1]).

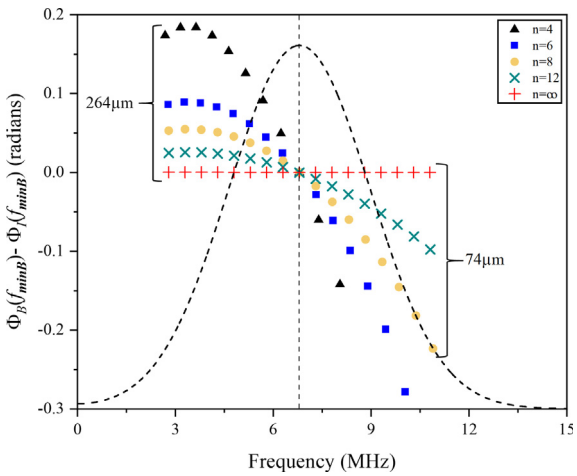

Fig. 6. Simulation results: the phase difference of the reflected signal and incident signal at f_{minB} under different thicknesses and the number of echoes. The vertical dashed black line represents the center frequency (6.8 MHz). To show the bandwidth of the transducer, the amplitude spectrum of the simulated incident signal is also plotted in arbitrary units using a red dash line.

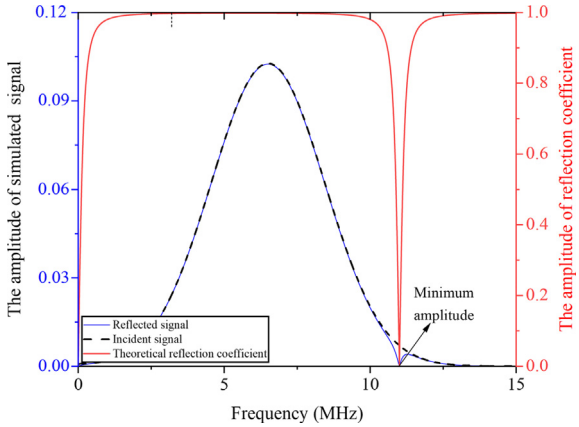

Fig. 7. Simulation results: variations of the simulated Amplitude spectrum of the reflected signal and theoretical amplitude spectrum of reflection coefficient when the minimum amplitude phenomenon first occurs in the border of the transducer bandwidth (the simulated oil film thickness is 67 μm), the peak frequency in the simulated amplitude of the reflected signal equals the actual.f_c

For the reflected signal in the blind zone, the oil film thickness can be determined by the phase model with the reconstructed phase of the incident signal. Meanwhile, the reflected signal from oil layers at different thicknesses are superposed in the time domain (see Fig. 8(b) in [1]), all the reflected echoes can be included directly to calculate the reflection coefficient. Therefore, the theoretical $|R(f)|$ can be calculated accurately using Eq. (6) rather than Eq. (11). Therefore, it is recommended that $|I(f)|$ should be reconstructed by using the $|B(f)|$ in the blind zone rather than the resonance model zone.

3.3. A schedule for the on-line reconstruction of the incident signal

To recover the phase and the amplitude of the incident signal, the spectrum of the reflected signal should be extracted from both the blind zone and the resonance model zone. That means the oil film thickness should be changed in a wide range to cover the two zones. Generally speaking, this can be accomplished by varying the running speed continuously in a sliding bearing which has a large working range of the oil film thickness [4,19].

The procedures for obtaining the incident signal are described as follows and the corresponding flowchart is shown in Fig. 8.

Step 1: Increase the oil film thickness by varying the relative speed of the tribo-pair until the resonance zone is identified from the reflected signals.

Step 2: Record the reflected signals consistently when increasing the oil film thickness.

Step 3: Transform the reflected signals into the frequency domain using the Fast Fourier transform algorithm (FFT). In this step, the full variation of $|B(f)|$ and $\Phi_B(f)$ can be obtained for subsequent processing.

Step 4: ① Scan $|B(f)|$ when the minimum amplitude phenomenon occurs at the border of ultrasonic bandwidth in $|B(f)|$, the peak frequency in $|B(f)|$ is extracted as the actual value of f_c.

② Scan $|B(f)|$ when the frequency of minimum amplitude approximates the actual f_c most in $|B(f)|$, the frequency of minimum amplitude is extracted (denoted as f_{minc}).

③ Extract the phase value of the reflected signal at f_{minc} as the phase of the incident signal at f_{minc} in the corresponding $\Phi_B(f)$.

Step 5: ① Use the extracted phase value of the incident value at f_{minc} to identify and extract the $|B(f)|$ in the blind zone and calculate its oil film thickness d by using the phase model (Eq. (7)).

② Calculate the theoretical $|R(f)_{n\to\infty}|$ at the oil film thickness d using Eq. (6).

③ Calculate $|I(f)|$ using Eq. (26).

4. Experimental validation

4.1. Experimental apparatus

The experiment apparatus is the same as those reported in [1,11,17,21]. The main part of the apparatus is the positioning rig, which consists of a stationary disk made of steel material, a movable disk made of steel material, and a micrometer. The thickness of the oil film between the stationary and the movable disks can be controlled by adjusting the movable disk with the micrometer. A 7 MHz ultrasonic transducer with a diameter of 7 mm is positioned at the rear end of the stationary disk using a standard strain gauge. By using the pulser-receiver, the ultrasonic transducer is excited and emits the ultrasonic pulse to the oil layer.

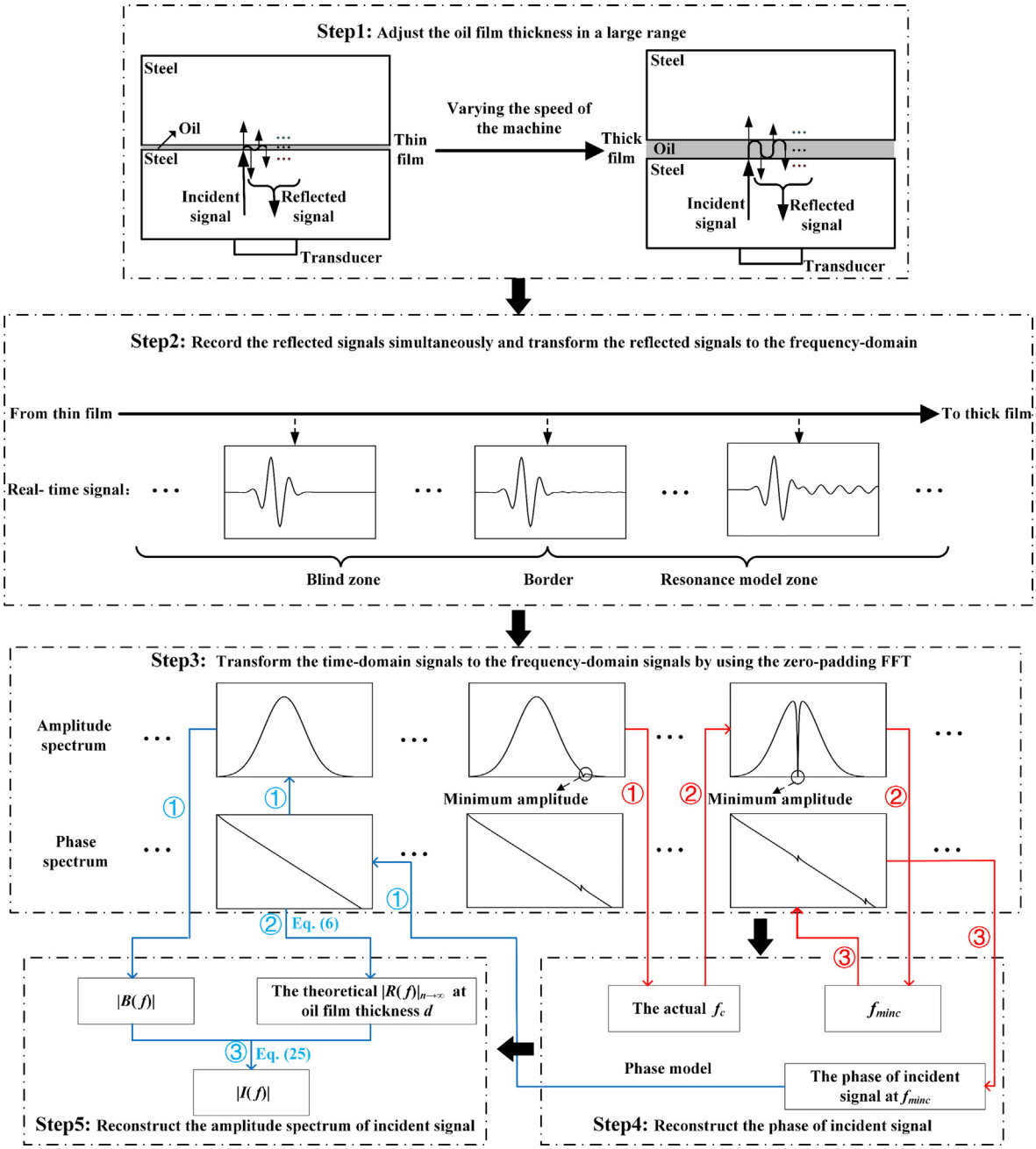

Fig. 8. The procedures of on-line reconstruction of the incident signal.

To compare the indirectly reconstructed incident signal, the reflected signal from the stationary disk-air interface was captured and stored as the actual incident signal. However, the actual measured incident signal fluctuated inherently in a certain range with the number of measurements due to the instability of pulser and receiver, electrical noise, acquisition, and trigger, etc. The fluctuation range of actual incident signal amplitudes and phase spectrums of 100 measurements was recorded and the averages of these actual incident signals were used as the final values.

Next, oil is evenly dropped on the surface of the stationary disk to form an oil film layer between the two disks. The oil film thickness can be changed continuously in a large range by adjusting the moveable disk with the micrometer. This process is to simulate the variation of oil film thickness in a real tribo-system.

4.2. Experiment procedures and results

By comparing with the actual incident signal, the reconstruction accuracy of the phase and amplitude of the incident signal is verified in subsection 4.2.1 and 4.2.2. Finally, the reconstruction algorithm of the incident signal is experimentally validated with the oil film thickness swept throughout the blind and resonance zones.

4.2.1. Reconstruction of the phase of the incident signal

The film thickness was swept from the spring model zone to the resonance model zone using the micrometer, with reflected signals collected simultaneously. When the minimum amplitude phenomenon occurs at the border of the bandwidth as shown in Fig. 9, $|B(f)|$ and $|I(f)|$ coincide basically in the vicinity of the center frequency. The peak frequency of the actual incident signal is often regarded as the actual f_c. In the enlarged view of Fig. 9, the peak frequency in the reflected signal is 6.52 MHz, which is basically equal to the actual f_c (6.54 MHz). The error mainly comes from the system noise. Therefore, the peak frequency can be approximated as the actual f_c.

Next, the oil film thickness was increased in the resonance model zone. Fig. 10 shows the Fourier transformed $|B(f)|$ and $\Phi(f)$ from oil layers at 84.80 μm, 108.51 μm, and 130.52 μm. It can be seen that the minimum amplitude phenomenon occurred in $|B(f)|$ due to the resonance phenomenon. In the corresponding $\Phi_B(f)$, the phase of the reflected signal is equal to that of the actual incident signal due to the resonance phenomenon.

The f_{minB} value in the amplitude spectrum of the reflected signal was extracted. Meanwhile, the reflection coefficient was calculated by the known reference signal, and the f_{minR} in the amplitude spectrum of the reflection coefficient was then extracted. By following the same steps as above, the f_{minR} and f_{minB} values at different oil film thicknesses can be obtained as shown in Fig. 11.

The overall trend of the frequency differences in Fig. 11 is that the values of f_{minR} - f_{minB} decrease as the resonance frequency in the x-axis increases. In particular, when f_{minB} is less than f_c, the frequency differences between the two increase considerably as the resonance frequency becomes smaller (see the green circled curve on the left of the vertical line in Fig. 11). When f_{minB} is equal to f_c, the frequency difference is close to zero. Fig. 11 also shows the relation of the calibration error of f_c and the deviation between the f_{minB} and f_{minR}. It can be seen that the deviation between f_{minB} and f_{minR} increases with a larger calibration error of f_c.

Then in $\Phi_B(f)$, the phase of reflected signals at minima frequencies was then extracted one by one. Fig. 12 shows the phase difference of the extracted phase to the phase of the actual incident signal at minima frequencies. The shaded area shows the fluctuation range of phase spectrums of the actual incident signal with 100 times of repeated measurements due to noise effect.

It can be seen that the phase difference is lowest and limited in the noise range when the frequency of minimum amplitude appears near the center frequency of the transducer. This is because the minimum frequency is equal to resonance frequencies at the actual center frequency. When the frequency of minimum amplitude is greater or lower than the center frequency, the phase difference increases in the negative and positive direction, respectively. The experimental result is consistent with the simulated result (see Fig. 6). In addition, it can be seen that when the frequency f_c is between 6.4 MHz and 6.8 MHz, the phase difference is limited in the range of −0.01 to 0.01 rad, which is acceptable as compared to the noise mag-

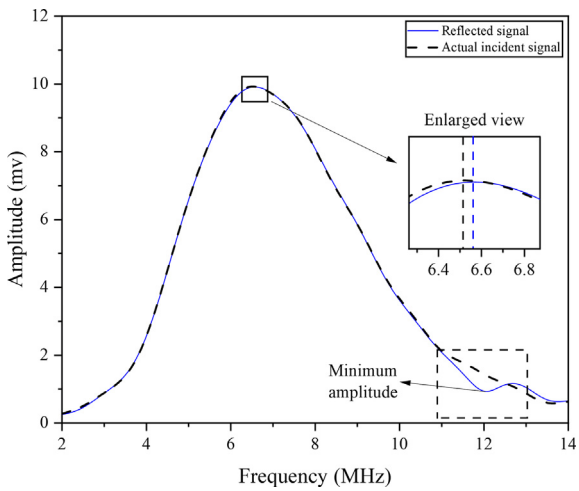

Fig. 9. Experimental results: the extraction of the actual f_c, the blue vertical line and black vertical line represent the position of the peak frequency of the reflected signal and actual incident signal in the enlarged view, respectively when the minimum amplitude phenomenon appears at the border, the peak frequency of reflected signal basically equal to the actual. f_c.

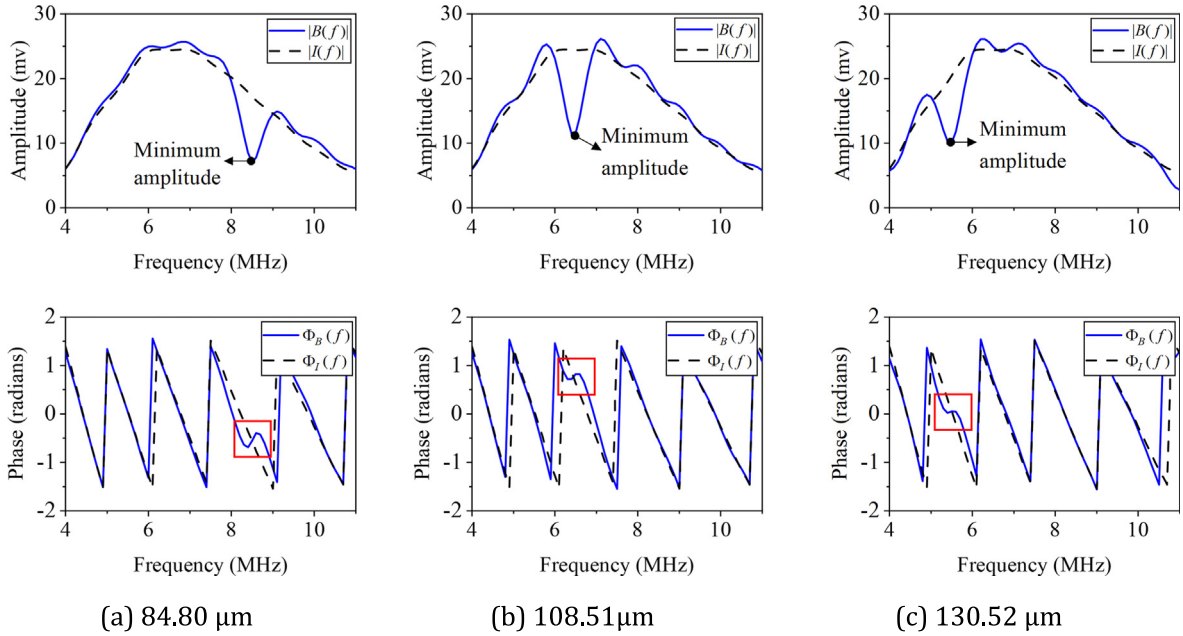

Fig. 10. The $|B(f)|$ and the $\Phi_B(f)$ from oil layers at 84.80 μm (a), 108.51 μm (b), and 130.52 μm (c), the phases of the reflected signal and the actual incident signal are equal at f_m in the red rectangular box.

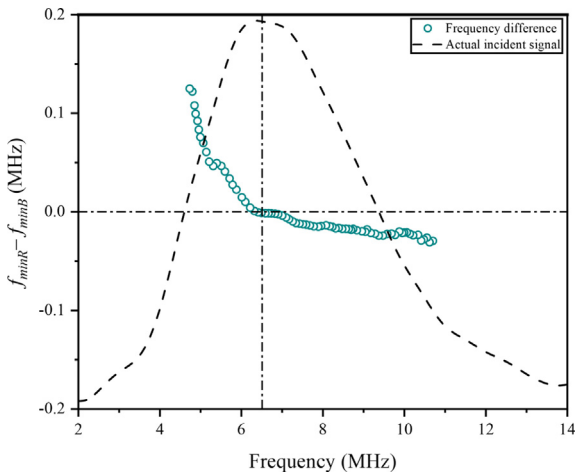

Fig. 11. The frequency differences of f_{minB} and f_{minR} at different resonance frequencies through experimental measurements, the vertical dash-dashed line represents the position of the center frequency (f_c), and the horizontal dash-dotted line represents the zero mark.

nitude. Finally, the phase of the reflected signal at the frequency of minimum amplitude approximating the 6.52 MHz is extracted as the phase of the incident signal.

4.2.2. Reconstruction of the amplitude spectrum of the incident signal

Then the identified phase of the incident signal was used to calculate the oil film thickness of the reflected signals below the first resonance. After that, $|B(f)|$ were used to calculate the $|I(f)|$ according to Eq. (26). Fig. 13 shows the calculated $|I(f)|$ (a) and corresponding relative error (b).

It can be seen that in the blind zone, the calculated $|I(f)|$ agree well with the actual one and relative errors are limited in the noise range. By comparison, the calculated results in the resonance model zone and spring model zone exist relatively high error. This is because, in the resonance model zone, the reflected signal was intercepted to calculate the amplitude spectrum and phase spectrum (see Fig. 8a in [1]). The number of echoes in the intercepted reflected signal is limited. However, the theoretical $|R(f)|$ in Eq. (26)is calculated by supposing that the number of echoes approaches infinity. Therefore, the error

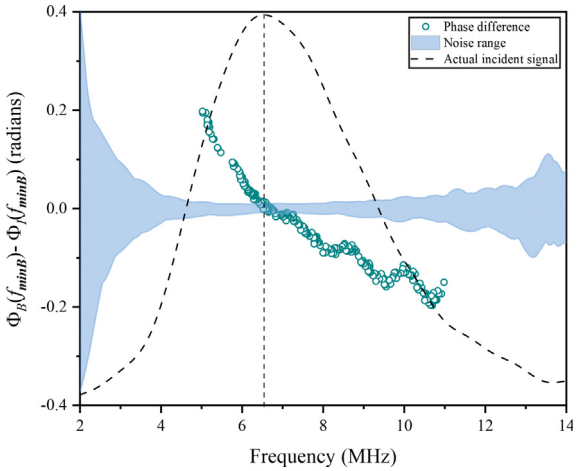

Fig. 12. Experimental results: the phase difference of the extracted phase to the phase of the actual incident signal at the minima frequencies, the dashed line represents the position of the center frequency when the minimum amplitude phenomenon appears at the center frequency, the phase of the reflected signal at f_c = 6.52 MHz equals that of the incident signal.

becomes high especially in the vicinity of the resonance frequency. In the spring model zone, the calculated oil film thickness by the spring model is sensitive to the rough surface (see Fig. 18 in [10]), thus leading to a large error.

4.2.3. Oil film thickness measurement

To demonstrate the effectiveness of the reconstruction algorithm of incident signal (namely Fig. 8), the micrometer is adjusted from thin oil film to thick oil film. Then the phase value and amplitude spectrum of the incident signal are reconstructed from reflected signals by using the reconstruction algorithm. After that, the film thickness is further reduced from thick oil film to thin film. The reconstructed phase value and amplitude spectrum of the incident signal are used to calculate the film thickness according to the phase model and the resonance model. During the whole process, the film thickness is also calculated by using the actual incident signal for comparison.

Fig. 14 shows the result of the four tests. The red colour represents the regular measurement by using the actual incident signal. The blue colour represents the auto-calibration measurement by using the reconstructed incident signal. The triangle and square represent the time when the phase value and amplitude spectrum are extracted indirectly in turn.

The result demonstrates that the measurement of film thickness by using the reconstructed incident signal agrees well with the one by using the actual incident signal. Especially in the resonance model zone and spring model zone, the results

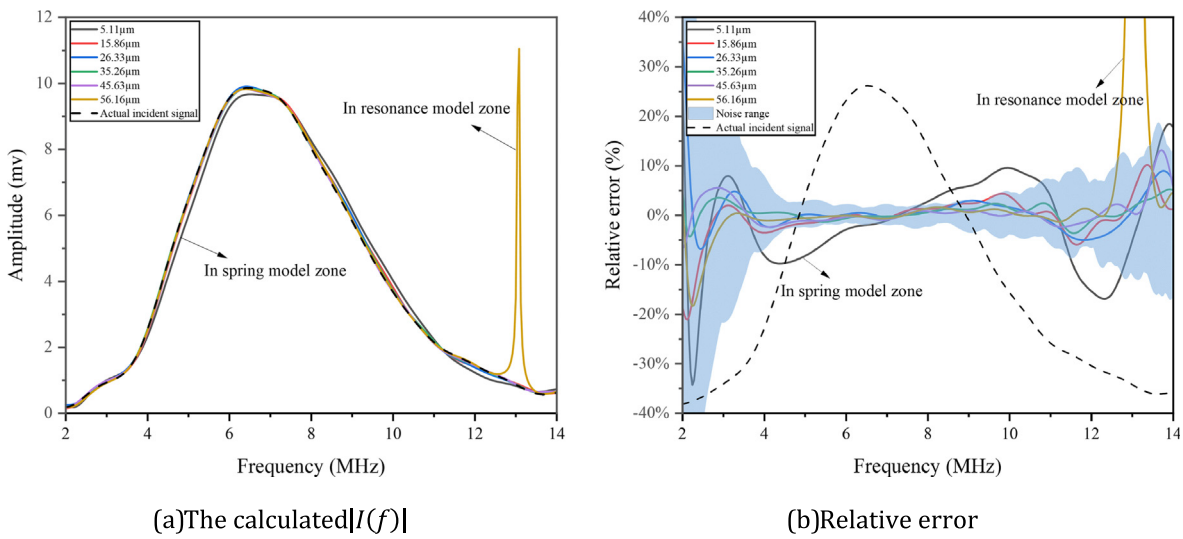

Fig. 13. Experimental results: the calculated $|I(f)|$ (a) and corresponding relative error (b), the shaded zone represents the noise range, the actual incident signal is also plotted in (b) at the arbitrary unit to show the bandwidth of transducer, the reconstructed error of $|I(f)|$ by using the $|B(f)|$ in the blind zone is accurate and basically limited in the noise range.

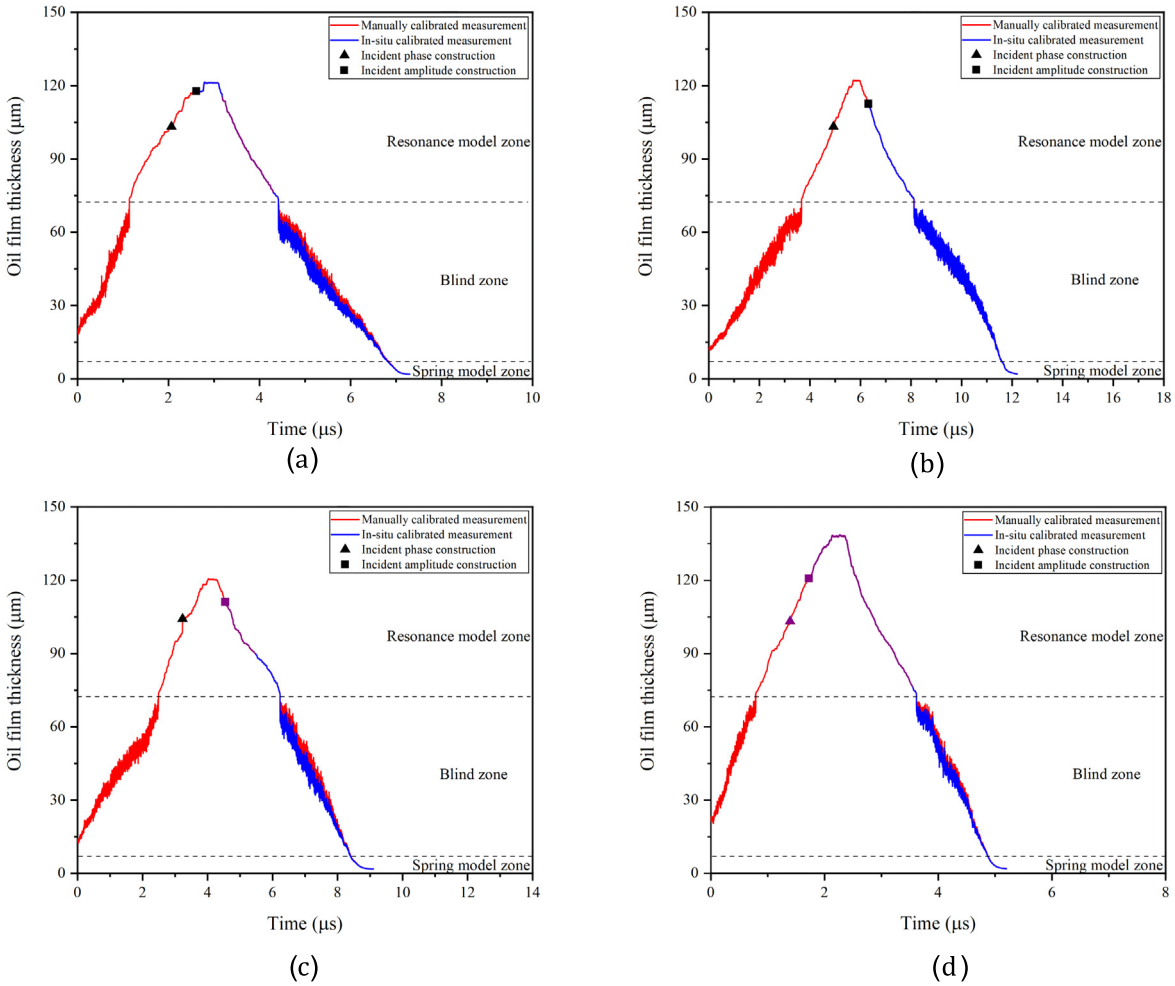

Fig. 14. Four measurements of oil film thickness using the actual incident signal (manually calibrated measurement) and the reconstructed incident signal (in-situ calibrated measurement) versus time as the micrometer was rotated to simulate the simultaneous change of film thickness, the black triangle and rectangular represent the moment that the phase and amplitude of the incident signal is constructed by using the reflected signals.

show high consistency and repeatability. By comparison, there exists high error relatively in the blind zone. This is because the phase model is sensitive to the phase of the incident signal (see Figs. 14 and 15 in [1]) and the reconstructed phase value will fluctuate inherently in the noise range, thus result in significant measurement uncertainties.

5. Discussion

Compared with the existing methods [10–14], the new reconstruction method of incident signal not only has a wide effective range, but also has high accuracy and repeatability. However, this technique requires that the oil film thickness in tribo-pairs needs to be swept in a wide range (at least between the blind zone and the resonance model zone) and the maximum film thickness needs to be adjusted in the tribo-pairs so that the minimum amplitude phenomenon can occur at the actual center frequency in $|B(f)|$.Table 1.

It can be seen in Fig. 15 that the maximum film thickness decreases with an increase in the center frequency. In practice, the transducer with a suitable center frequency can be selected according to the adjustable range of film thickness in the actual machine. For example, if the estimated adjustable range of oil film thickness in the actual machine is 0 ~ 70 μm, the suggested center frequency is above 10 MHz. In addition, the signal attenuation may not be ignored when the center frequency increases. Therefore, the penetration depth of the sonic wave should be taken into the consideration.

Table 1
Properties of different materials in three-layered structures.

Material	Density ($kg \cdot m^{-3}$)	Acoustic speed ($m \cdot s^{-1}$)	Acoustic impedance (10^6 $kg \cdot m^{-2} \cdot s^{-1}$)
oil	886	1467	1.27
steel	5818	7810	45.4

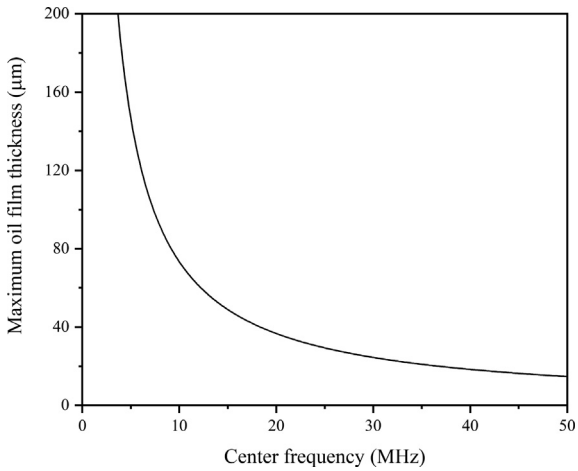

Fig. 15. Maximum film thickness as a function of the center frequency.

6. Conclusion

To obtain the incident signal in ultrasonic-based oil film thickness measurement without disassembling the tribo-pair, a new approach for reconstructing the incident signal from the reflected signal is presented in this paper.

First, the relationship between the reflected signal and the incident signal is analyzed in the resonance model zone. It is found that the phase of the reflected signal is equal to the phase of the incident signal at the frequency of minimum amplitude when the frequency of minimum amplitude occurs at the actual center frequency. Based on this phenomenon, the phase of the incident signal can be reconstructed from the phase of the reflected signal. By using the extracted phase of the incident signal, the reflected signal in the blind zone can be identified and its amplitude spectrum can be used to calculate the amplitude spectrum of the incident signal. Finally, a reconstruction algorithm of the incident signal is proposed to extract the amplitude and the phase of the incident wave when the oil film thickness varies in the resonance and the blind zone.

The accuracy of the proposed method was verified experimentally with controlled oil film thickness. Results showed that the reconstructed phase and amplitude of the incident signal agree well with that measured directly and the error was basically bounded within the noise range. Measurement results of film thickness using the reconstructed incident signal maintain identical accuracy basically with the manually calibrated measurement. However, this technique requires that the thickness of the oil film in tribo-pairs can be widely swept to cover both the blind and resonance zones. For example, when a 10 MHz ultrasonic transducer is utilized, the oil film thickness needs to be swept from 50 μm to 70 μm, which is possible for sliding bearing. In addition, the robustness of the method also needs to be improved because any interference changing the incident signal would require another calibration procedure, which may limit the implementation of this method in a running machine. In the future, more experimental validation in the real hydromantic applications will be conducted.

CRediT authorship contribution statement

Pan Dou: Methodology, Software, Validation, Writing - original draft. **Yaping Jia:** Investigation. **Tonghai Wu:** Supervision. **Zhongxiao Peng:** Writing - review & editing. **Min Yu:** Writing - review & editing. **Tom Reddyhoff:** Writing - review & editing.

Declaration of Competing Interest

The authors declare that they have no known competing financial interests or personal relationships that could have appeared to influence the work reported in this paper.

Acknowledgments

The authors appreciate the financial support from the National Natural Science Foundation of China (No. 51975455 and No. 51675403) and the support of K. C. Wong Education Foundation.

References

[1] P. Dou, T. Wu, Z. Luo, Wide range measurement of lubricant film thickness based on ultrasonic reflection coefficient phase spectrum, J. Tribol. 141 (2019), https://doi.org/10.1115/1.4041511.
[2] T. Pialucha, P. Cawley, The detection of thin embedded layers using normal incidence ultrasound, Ultrasonics. 32 (6) (1994) 431–440, https://doi.org/10.1016/0041-624X(94)90062-0.
[3] T. Pialucha, C.C.H. Guyott, P. Cawley, Amplitude spectrum method for the measurement of phase velocity, Ultrasonics. 27 (5) (1989) 270–279, https://doi.org/10.1016/0041-624X(89)90068-1.
[4] R.S. Dwyer-Joyce, B.W. Drinkwater, C.J. Donohoe, The measurement of lubricant-film thickness using ultrasound, Proc. R. Soc. A Math. Phys, Eng. Sci. 459 (2032) (2003) 957–976, https://doi.org/10.1098/rspa.2002.1018.
[5] R.S. Dwyer-Joyce, P. Harper, B.W. Drinkwater, A method for the measurement of hydrodynamic oil films using ultrasonic reflection, Tribol. Lett. 17 (2) (2004) 337–348, https://doi.org/10.1023/B:TRIL.0000032472.64419.1f.
[6] H.G. Tattersall, The ultrasonic pulse-echo technique as applied to adhesion testing, J. Phys. D. Appl. Phys. 6 (1973) 819–832, https://doi.org/10.1088/0022-3727/6/7/305.
[7] M. Yu, L.i. Shen, T. Mutasa, P. Dou, T. Wu, T. Reddyhoff, Exact analytical solution to ultrasonic interfacial reflection enabling optimal oil film thickness measurement, Tribol. Int. 151 (2020) 106522, https://doi.org/10.1016/j.triboint.2020.106522.
[8] B. Praher, G. Steinbichler, Ultrasound-based measurement of liquid-layer thickness: A novel time-domain approach, Mech. Syst. Signal Process. 82 (2017) 166–177, https://doi.org/10.1016/j.ymssp.2016.05.016.
[9] P. Dou, T. Wu, Z. Peng, A time-domain ultrasonic approach for oil film thickness measurement with improved resolution and range, Meas. Sci. Technol. 31 (7) (2020) 075006, https://doi.org/10.1088/1361-6501/ab7a69.
[10] A. Hunter, R. Dwyer-Joyce, P. Harper, Calibration and validation of ultrasonic reflection methods for thin-film measurement in tribology, Meas. Sci. Technol. 23 (10) (2012) 105605, https://doi.org/10.1088/0957-0233/23/10/105605.
[11] T. Geng, Q. Meng, X. Xu, P. Wang, X. Yuan, An extended ultrasonic time-of-flight method for measuring lubricant film thickness, Proc. Inst. Mech. Eng. Part J J. Eng. Tribol. 229 (7) (2015) 861–869.
[12] T. Reddyhoff, R.S. Dwyer-Joyce, J. Zhang, B.W. Drinkwater, Auto-Calibration of Ultrasonic Lubricant-Film Thickness Measurements, Meas. Sci. Technol. 19 (4) (2008) 045402, https://doi.org/10.1088/0957-0233/19/4/045402.
[13] R.L. Kaeseler, P. Johansen, Adaptive ultrasound reflectometry for lubrication film thickness measurements, Meas. Sci. Technol. 31 (2) (2020) 025108, https://doi.org/10.1088/1361-6501/ab35f2.
[14] J. Jiao, W. Liu, J. Zhang, Q. Zhang, C. He, B. Wu, Time–frequency analysis for ultrasonic measurement of liquid-layer thickness, Mech. Syst. Signal Process. 35 (1-2) (2013) 69–83, https://doi.org/10.1016/j.ymssp.2012.08.015.
[15] T. Reddyhoff, S. Kasolang, R.S. Dwyer-Joyce, B.W. Drinkwater, The phase shift of an ultrasonic pulse at an oil layer and determination of film thickness, Proc. Inst. Mech. Eng. Part J J. Eng. Tribol. 219 (2005).
[16] L. Brekhovskikh, Waves in layered media, Elsevier, 2012.
[17] P. Dou, T. Wu, Z. Luo, Z. Peng, T. Sarkodie-Gyan, The application of the principle of wave superposition in ultrasonic measurement of lubricant film thickness, Meas. J. Int. Meas. Confed. 137 (2019) 312–322, https://doi.org/10.1016/j.measurement.2019.01.057.
[18] R. Demirli, J. Saniie, Model-based estimation of ultrasonic echoes. Part I: Analysis and algorithms, IEEE Trans. Ultrason. Ferroelectr. Freq. Control. 48 (3) (2001) 787–802, https://doi.org/10.1109/58.920713.
[19] S.B. Glavatskih, D.M.C. McCarthy, I. Sherrington, Further transient test results for a pivoted-pad thrust bearing, in: G. Dalmaz, A.A. Lubrecht, D. Dowson, M. Priest (Eds.), Transient Process. Tribol., Elsevier, 2003: pp. 301–312. https://doi.org/10.1016/S0167-8922(03)80058-5
[20] S. Kasolang, R.S.D. Joyce, M.A. Ahmad, PZT transducer design and pulsing optimization for film thickness and viscosity measurement, Sensors Actuators A Phys. 203 (2013) 386–393, https://doi.org/10.1016/j.sna.2013.08.039.
[21] J. Zhang, B.W. Drinkwater, R.S. Dwyer-Joyce, Calibration of the ultrasonic lubricant-film thickness measurement technique, Meas. Sci. Technol. 16 (2005) 1784–1791, https://doi.org/10.1088/0957-0233/23/10/105605.